Journal of Power Sources 195 (2010) 2507–2513

Contents lists available at ScienceDirect

Journal of Power Sources

journal homepage: www.elsevier.com/locate/jpowsour

Enhancement of catalytic activity of platinum-based nanoparticles towards electrooxidation of ethanol through interfacial modification with heteropolymolybdates

Piotr J. Barczuk, Adam Lewera, Krzysztof Miecznikowski, Artur Zurowski, Pawel J. Kulesza*

Department of Chemistry, University of Warsaw, Pasteura 1, PL-02-093 Warsaw, Poland

ARTICLE INFO

Article history:
Received 21 May 2009
Received in revised form 20 October 2009
Accepted 16 November 2009
Available online 22 November 2009

Keywords:
Electrocatalysis
Ethanol oxidation
Bimetallic Pt–Ru and Pt–Sn nanoparticles
Polyoxometallate layers

ABSTRACT

As evidenced from the increase of electrocatalytic currents measured under voltammetric and chronoamperometric conditions, the activity of bimetallic Pt–Ru and Pt–Sn nanoparticles towards oxidation of ethanol is increased by modification of their surfaces with ultra-thin films of phosphododecamolybdic acid ($H_3PMo_{12}O_{40}$). The enhancement effect has been most pronounced in a case of heteropolymolybdate-modified carbon-supported Pt–Sn catalysts. Independent high-resolution XPS measurements indicate the ability of heteropolymolybdates to stabilize tin (in bimetallic Pt–Sn particles) at higher oxidation states (presumably as tin oxo species). The overall activation effect may also be ascribed to changes in the morphology of catalytic films following modification with heteropolymolybdates. Presence of the polyoxometallate is also likely to increase of the interfacial population of reactive oxo groups in the vicinity of platinum centers.

1. Introduction

Low-temperature alcohol fuel cells can be considered as alternatives to hydrogen-utilizing systems. Direct methanol fuel cells have so far been the most extensively studied, and they are characterized by reasonable efficiencies. Nevertheless, methanol as a fuel has several disadvantages including its toxicity. Ethanol is much less toxic, and it may be obtained from renewable (biomass) resources. But electrooxidation of ethanol is a much more complex process, and the reaction mechanism requires cleavage of C–C bond in the C_2H_5OH molecule. Thus the reaction rate is very low at ambient conditions [1–3]. Among noble metals platinum shows the highest activity towards dissociative adsorption of organic molecules at low temperatures. But the platinum surface is immediately poisoned with by-products (including carbon monoxide) formed during the ethanol electrooxidation process. In a case of the methanol system, the latter problem is largely solved with use of bimetallic Pt–Ru alloys or Ru-decorated Pt catalysts. Ruthenium shows capability of activation of interfacial water molecules through creating the adsorbed –OH groups that are highly reactive towards oxidation of CO residues to CO_2 [4–7]. Because electrooxidation of ethanol would require first breaking of C–C bonds followed by removing poisoning species (adsorbates), the effective electrocatalytic system would certainly be much more complex. An interesting possibility arises from modification of platinum surface (or from designing the environment around it) to promote activating interactions of Pt centers with the second additive. There have been a few bi- and tri-metallic electrocatalytic systems proposed in literature for ethanol oxidation [8–11]. Nevertheless it is usually accepted that the best electrocatalytic performance for oxidation of ethanol is obtained with use of Pt–Sn catalysts [12–15]. But the overall efficiencies of Pt–Sn type anodes are rather low relative not only to fuel cells based on hydrogen oxidation but also when compared to systems utilizing electrooxidation of methanol (e.g. at Pt–Ru catalysts) [16]. While methanol undergoes oxidation to CO_2 as a final product, main products of the ethanol reaction are acetic acid and acetaldehyde rather than carbon dioxide.

In the present paper, we address the influence of ultra-thin films of Keggin-type heteropolymolybdates ($PMo_{12}O_{40}^{3-}$) on catalytic activity of Pt, Pt–Ru and Pt–Sn nanoparticles during electrooxidation of ethanol. In addition to such interesting properties as photoactivity [17], electrochromism [17] and high acidity [18], the usefulness of heteropolymolybdates in electrocatalysis [19,20] has also been established. Heteropolyacids of molybdenum and tungsten are known to form nanocomposite materials capable of inducing electrooxidation of methanol [20] or electroreduction of oxygen [21–23].

Ultra-thin films or adsorbates of heteropolymolybdates or tungstates have not only been found to activate catalytic noble metal (Pt) nanoparticles but also to protect them from agglomeration, namely through electrostatic repulsion between negatively

* Corresponding author. Tel.: +48 8220211x289; fax: +48 8225996.
E-mail address: pkulesza@chem.uw.edu.pl (P.J. Kulesza).

0378-7753/$ – see front matter © 2009 Elsevier B.V. All rights reserved.
doi:10.1016/j.jpowsour.2009.11.066

charged monolayers on their surfaces [21,24,25]. Another important feature is that adsorbates of such spacious heteropoly molecules seem to occupy only a very small fraction (a few percent) of interfacial Pt atoms, and they seem not to block access of reactants to catalytic Pt sites [21]. Further, they are characterized by fast electron transfers facilitating electronic communication between the electrode surface and catalytic sites [23]. Finally, our interest in polymolybdates has been dictated by the recent findings clearly indicating the activating role of molybdenum (existing in the vicinity of platinum) on electrooxidation of ethanol [26].

Three different catalytic systems, such as bare Pt, as well as bimetallic Pt–Ru and Vulcan-supported Pt–Sn (Pt–Sn/C) nanoparticles have been modified with ultra-thin films of phosphododecamolybdates (PMo_{12}). We consider here simple Pt nanoparticles as a model electrocatalyst, or a standard for comparison, that should allow us to comment unequivocally on nature of the activation effect originating from PMo_{12}. Among all systems studied, the overall enhancement effect has been the most pronounced in a case of Pt–Sn/C nanoparticles. High-resolution XPS studies of the latter system (performed before and after modification with PMo_{12}) have given us some insight into electronic interactions and roles of particular catalytic components. For example, it was demonstrated previously for the Ru/Se-type oxygen reduction catalysts that Se-overlayer was capable of draining electrons from Ru-core and thus making the metal less susceptible to oxidation even at higher potentials [27,28]. In the present case of the ethanol oxidation, we have addressed importance of the chemical identity of tin [29,30] in the overall electrocatalytic activity of the Pt–Sn/C system.

2. Experimental

All chemicals were commercially available materials of the analytical grade purity. Phosphododecamolybdic acid ($H_3PMo_{12}O_{40}$), PMo_{12}, was obtained from Aldrich. Catalytic Pt and Pt–Ru nanoparticles (1:1 alloy) were obtained from Alfa Aesar. Vulcan-supported Pt–Sn/C nanoparticles (20% metal loading relative to Vulcan; Pt:Sn ratio, 3:1) were purchased from E-TEK. Solutions were prepared using doubly distilled and subsequently de-ionized (Millipore Milli-Q) water. Argon was used to de-aerate solutions and to keep air-free atmosphere over the solution during measurements.

Morphology of catalytic particles was monitored using Philips CM10 scanning transmission microscope (TEM) operating at the voltage of 100 kV. Samples for TEM measurements were prepared by placing colloidal solutions of nanoparticles on grids and, subsequently, subjecting them to drying.

All electrochemical measurements were performed in three-electrode configuration using CH Instruments 660B and 600B workstations. The K_2SO_4-saturated Hg/Hg_2SO_4 was the reference electrode; and a carbon rod was used as the counter electrode. All potentials have been recalculated and expressed versus the reversible hydrogen electrode (RHE).

Working electrodes were fabricated through modification of glassy carbon substrates (diameter, 3 mm) with Pt, Pt–Ru or Pt–Sn/C nanoparticles. Inks of these particles were prepared as follows: 400 μl of ethanol and 80 μl of 5% solution of Nafion were added to 5.5 mg sample of the respective nanoparticles. Such solution was stirred for 12 h. Then 3 μl of the solution was placed onto the surface of glassy carbon electrode and, then, it was left to dry. The resulting electrodes were activated through potential cycling in 0.5 mol dm^{-3} H_2SO_4 in the following ranges of potentials: from 0 to 0.95 V and from 0 to 0.5 V for Pt, or Pt–Ru, and Pt–Sn/C, respectively. The total loading of metallic nanoparticles was equal to 0.49 mg cm^{-2} in each case. Interfacial modification with ultra-thin films of PMo_{12} was achieved by immersing the respective electrode covered with assembled nanoparticles (as described above) into the 0.005 mol dm^{-3} PMo_{12} solution for 15 min. Later, the resulting electrode material was subjected to rinsing with distilled water to remove excessive (unbound) PMo_{12}.

Preparation of the PMo_{12}-modified Pt–Sn/C nanoparticles suitable for XPS measurements was done as follows: 27.5 mg of Pt–Sn/C (5.5 mg of pure Pt–Sn nanoparticles) was dispersed within 400 μl of aqueous 0.005 mol dm^{-3} $H_3PMo_{12}O_{40}$. The suspension was subsequently sonicated for 24 h and, later, centrifuged. Then supernatant solution was replaced with fresh heteropolyacid solution, and the above procedure was repeated. To produce stable colloidal suspensions of modified Pt–Sn/C particles, the above sonication and centrifuging steps were repeated 3–4 times in water.

High-resolution synchrotron XPS measurements were performed at Bessy-II (Berlin, Germany) using the undulator beamline U49/2-PGM 2 at the SoLiAS end station at 650 eV photon energy. PMo_{12}-stabilized nanoparticles were deposited onto a gold disk and dried in ambient atmosphere, as described before [31]. The spectra were calibrated with respect to Fermi-edge and bulk Au 4*f* signal for each experiment at the given excitation energy. The standard error for core-level binding energies was estimated to be below 0.03 eV.

3. Results and discussion

3.1. Physicochemical identity of catalytic nanoparticles

Fig. 1 illustrates transmission electron microscopy (TEM) images of (A) Pt, (B) Pt–Ru and (C) Pt–Sn/C nanoparticles utilized in the present work. Both Pt and Pt–Ru nanoparticles that according to the manufacturer's specification and our previous observations [20–24] should be below 10 nm, tend to form agglomerates (Fig. 1A and B). For example, it is clear from Fig. 1A that Pt nanocrystallites (typically <10 nm) coalesce with one another. Pt–Ru nanoparticles (dark spots) are definitely amorphous, their sizes differ from 2 to 10 nm, and they are dispersed (Fig. 1B). Also Vulcan (carbon)-supported Pt–Sn (Pt–Sn/C) nanostructures exist as agglomerates (Fig. 1C). In addition to linked units of 30–40 nm (presumably characteristic of Vulcan supports), careful examination of the latter system permits distinguishing darker spots of sizes of a few nanometers that shall be attributed to bimetallic Pt–Sn nanoparticles. On the whole, appearance of large agglomerates under conditions of the present TEM microscopic measurements does not imply the existence of analogous morphologies during operation of catalysts when deposited on the electrode surface (for diagnostic voltammetric experiments) or on the Nafion membrane in a fuel cell.

Following deposition of the Nafion-containing inks of our catalytic systems (Pt, Pt–Ru and Pt–Sn/C) on glassy carbon electrode substrates, the respective voltammetric responses (Fig. 2) were recorded in 0.5 mol dm^{-3} H_2SO_4 before (solid lines) and after (dotted lines) modification with PMo_{12}. Presence of adsorbates or ultra-thin films of PMo_{12} on glassy carbon was evident from appearance of the peaks characteristic of the PMo_{12} redox reactions [22,32]. In the simplified form, they can be described as follows:

$$PMo_{12}{}^{VI}O_{40}{}^{3-} + ne^- + 6H^+ \rightarrow H_nPMo_n{}^{V}Mo_{12-n}{}^{VI}O_{40}{}^{3-} \quad (1)$$

The PMo_{12} adsorbate exhibited typical reversible two-electron redox processes [32] when it was deposited on Pt–Sn/C (Fig. 2C). In cases of Pt and Pt–Ru nanoparticles (Fig. 2A and B), the voltammetric peaks of PMo_{12} layers tended to overlap each other to produce broad peak signals. The existence of clearly separated PMo_{12} voltammetric peaks in Fig. 2C may originate from presence of carbon (Vulcan) support onto which PMo_{12} is preferentially adsorbed. Our previous electrochemical [24,25,33,34] and FTIR measurements [35,36] clearly demonstrate that PMo_{12}

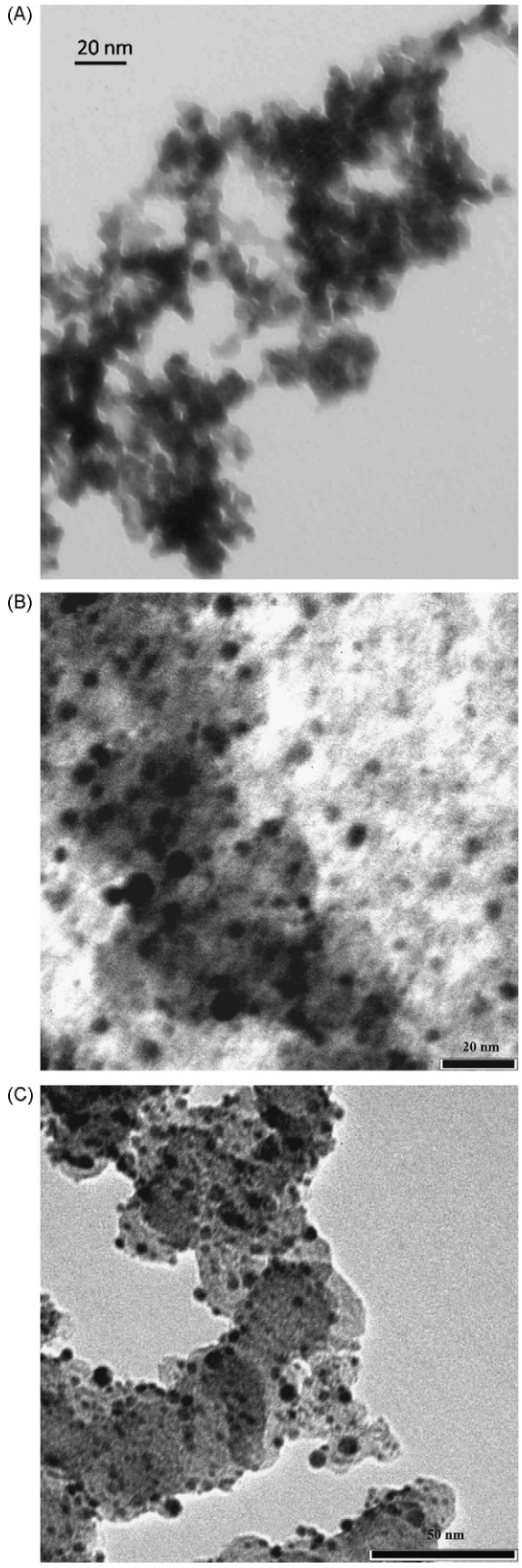

Fig. 1. Transmission electron micrographs (TEMs) of (A) Pt; (B) Pt–Ru; and (C) Pt–Sn/C nanoparticles.

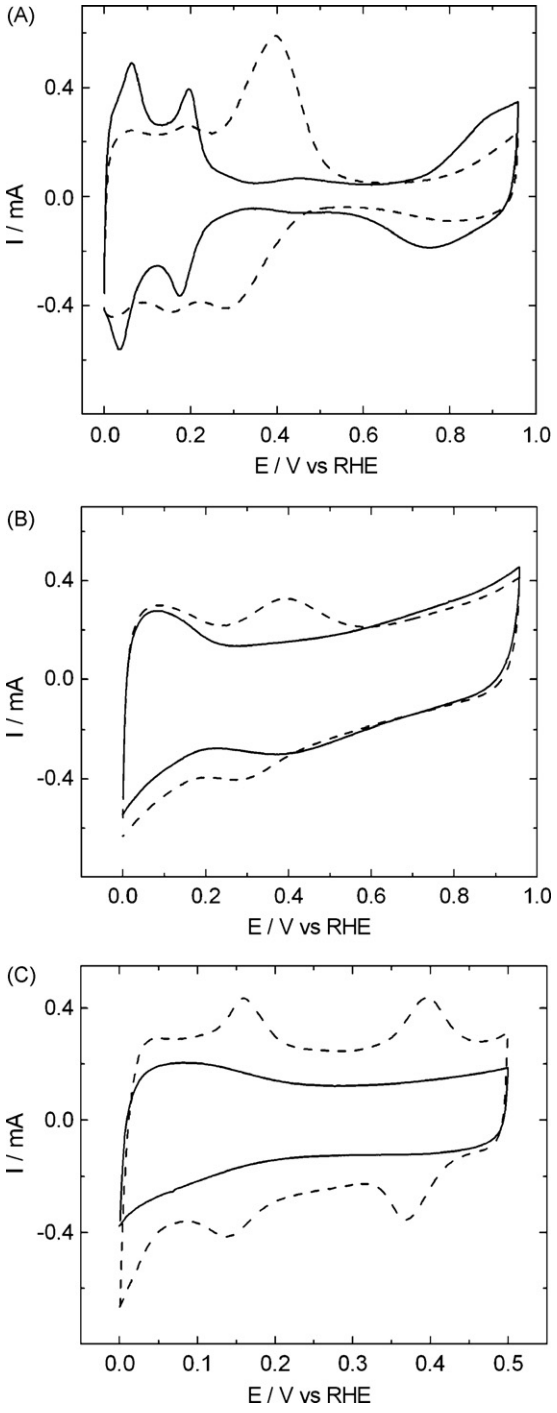

Fig. 2. Cyclic voltammetric responses of (A) Pt; (B) Pt–Ru; and (C) Pt–Sn/C catalytic systems together with (dashed lines) and without (solid lines) ultra-thin films PMo_{12}. Electrolyte: 0.5 mol dm^{-3} H_2SO_4. Scan rate: 50 mV s^{-1}.

is strongly chemisorbed on carbon nanostructures, as well as it retains its model redox behavior and its physicochemical identity. Redox characteristics of PMo_{12} adsorbates on Pt-based nanostructures are expected to be more complex because the system voltammetric behavior is affected by presence of hydrogen adsorption/desorption peaks on Pt and by the substrate oxidation to various Pt oxo species. As expected from the previous studies [21], in comparison to bare Pt nanoparticles, their modification with PMo_{12} results in partial suppression of the formation of platinum oxides at potentials higher than 0.6 V (Fig. 2A). No potential excursions have been made towards such positive values in the case

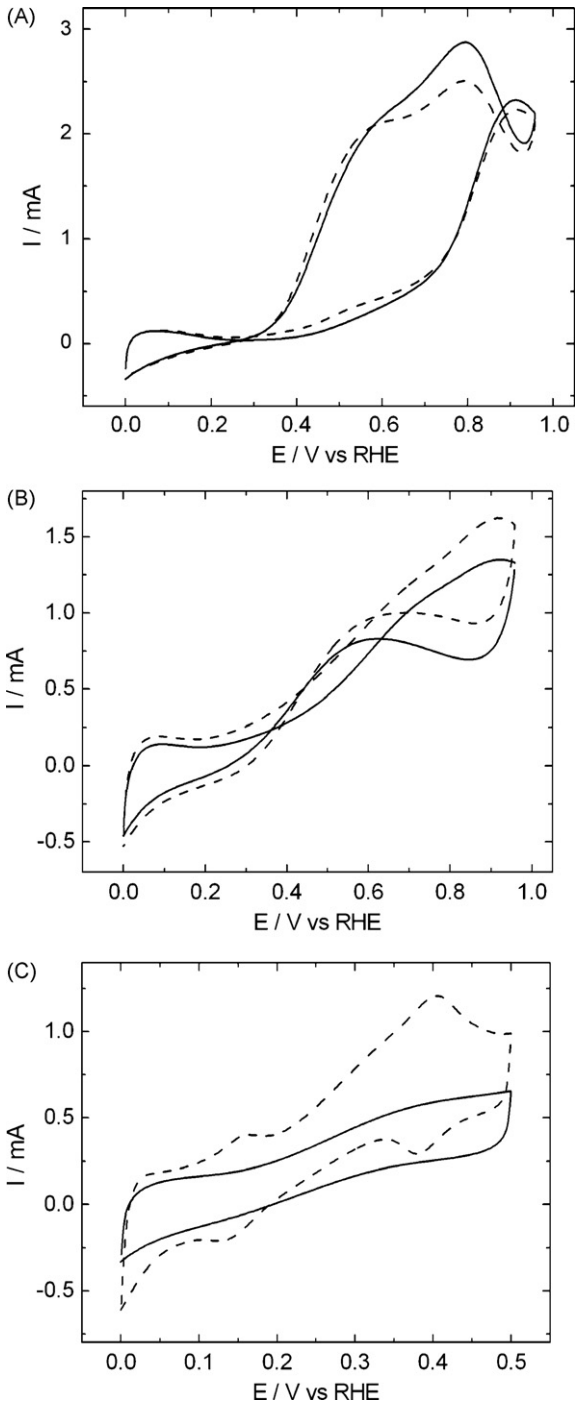

Fig. 3. Voltammetric oxidation of 0.5 mol dm^{-3} ethanol at (A) Pt; (B) Pt–Ru; and (C) Pt–Sn/C catalytic systems covered with (dashed lines) and without (solid lines) ultra-thin films PMo_{12}. Electrolyte: 0.5 mol dm^{-3} H_2SO_4. Scan rate: 50 mV s^{-1}.

of Pt–Sn/C nanoparticles because of danger of their degradation (corrosion of tin).

3.2. Electrooxidation of ethanol

Fig. 3 illustrates representative cyclic voltammetric responses of our catalytic systems recorded in the 0.5 mol dm^{-3} ethanol (in 0.5 mol dm^{-3} H_2SO_4 electrolyte) solution. First, the measurements were performed using unmodified nanoparticles of (A) Pt, (B) Pt–Ru, and (C) Pt–Sn/C (Fig. 3, solid lines). Later, the same systems were modified with PMo_{12} and subjected to voltammetric investigations (Fig. 3, dotted lines). Despite some irreproducibility in the recorded voltammetric electrocatalytic data, the results of Fig. 3 are typical and reproducible. Following adsorption of PMo_{12}, all examined electrodes exhibited higher (certainly not lower) voltammetric electrocatalytic currents during oxidation of ethanol at the potentials lower than 0.5 V, i.e. in the potential range crucial from the viewpoint of potential applications in fuel cells. The fact that the PMo_{12}-modified Pt system tended to show somewhat lower electrocatalytic activity at potentials higher than 0.5 V (Fig. 3A) may have origin in the different morphology of PtOH or PtO species generated on platinum in the presence and absence of the polyoxometallate overlayer. The largely suppressed character of voltammetric responses (Fig. 2A, dotted line) related to the formation of Pt oxides (in H_2SO_4) in the presence of PMo_{12} (that is not electroactive at potentials higher than 0.5 V) may be caused by difficulties in charge propagation within the presumably robust and compact structures of PMo_{12}-modified oxides. Such restrictions could exhibit an inhibiting effect in electrocatalysis (Fig. 3A, dotted line). Further, it is reasonable to expect some chemical (due to oxidizing capabilities of PMo_{12}), interactions between polymolybdate and ruthenium or tin components of bimetallic Pt–Ru or Pt–Sn catalysts. Thus different characteristics of the latter systems during electrocatalytic oxidations of ethanol are not surprising (Fig. 3B and C).

There is always competition between the activating role of the additive (PMo_{12}) and its physical blocking of Pt active sites. Bare platinum has high capability of adsorbing and inducing electrochemical decomposition of the organic molecule (ethanol). On the other hand – without additives – the metal would be readily poisoned by adsorbing reactant or reaction intermediates (carbon monoxide). Modification of Pt–Ru nanoparticles with PMo_{12} has certainly resulted in their some activation towards oxidation of ethanol (Fig. 3B). Nevertheless, the largest enhancement of electrocatalytic currents has been observed in the case of Pt–Sn/C catalyst (Fig. 3C). It is noteworthy that we limit here our investigations to potentials not exceeding 0.5 V to avoid any possible dissolution of tin component in Pt–Sn. The simplest explanation of the above observation would take into account possible activity of PMo_{12} and its ability to adsorb not only on metal (Pt–Sn) nanoparticles but also on the nanostructured carbon supports. The presence of carbon support also provides high surface area and permits accumulation of larger amounts of PMo_{12} in the vicinity of the catalytic (Pt–Sn) metal nanoparticles. Electroactivity of PMo_{12} is clearly visible from the appearance of two pairs of reversible peaks not only in supporting electrolyte (Fig. 2C) but also during electrooxidation of ethanol (Fig. 3C). While mediating (electron transfer) capabilities of PMo_{12} can easily be envisioned at potentials below 0.5 V (Fig. 2C), it is difficult to postulate – on basis of the present data – a direct chemical involvement of PMo_{12} in the overall ethanol electrooxidation mechanism (despite previous reports postulating enhancement of the electrocatalytic oxidation of methanol in the presence of molybdates [37]).

To get more insight into activity of the proposed electrocatalytic systems during oxidation of ethanol, we have performed chronoamperometric measurements (Figs. 4 and 5) at two different potentials, 0.3 and 0.4 V, respectively. In all cases, modification of all systems utilizing PMo_{12}-modified metal nanoparticles leads to evident increases of catalytic currents under chronoamperometric conditions (compare dotted and solid lines in Figs. 4 and 5). As expected from the voltammetric data (Fig. 3), the enhancement effect has been the most pronounced for Pt–Sn/C nanoparticles.

To comment on prolonged stability of the electrocatalytic responses in the presence of ethanol, the long-term chronoamperometric measurements (at 0.4 V) with the optimum PMo_{12}-modified Pt–Sn/C system have been performed (Fig. 6, dotted line). Comparison has been made to bare (PMo_{12}-unmodified) Pt–Sn/C

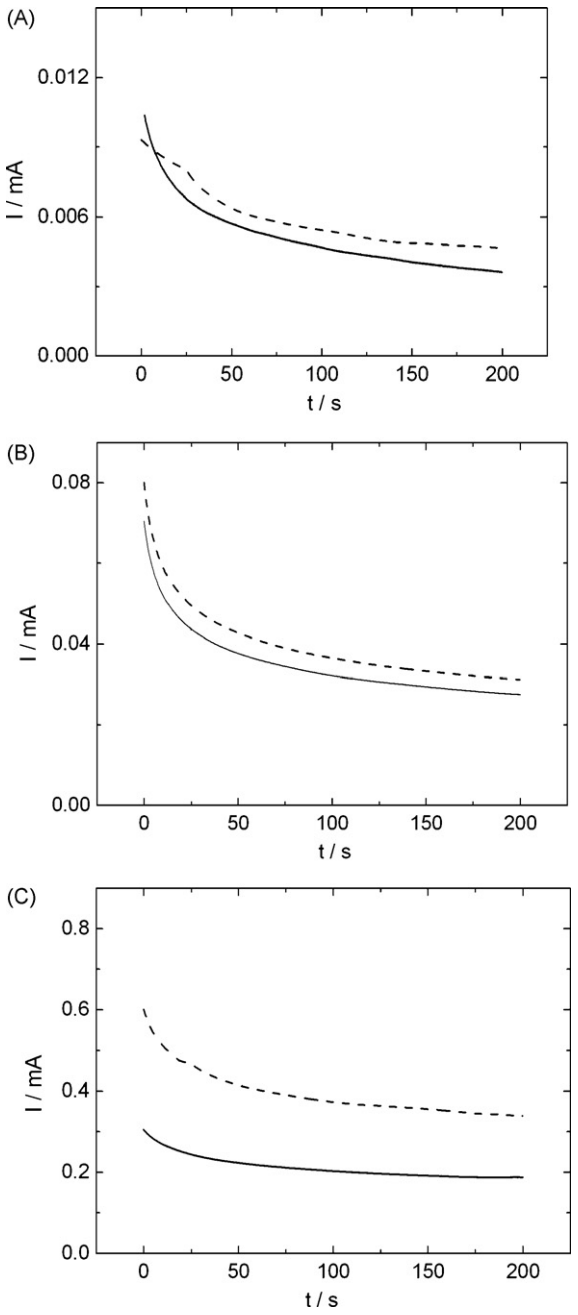

Fig. 4. Chronoamperometric responses recorded at 0.3 V for the oxidation of 0.5 mol dm^{-3} ethanol at (A) Pt; (B) Pt–Ru; and (C) Pt–Sn/C nanoparticles covered with (dashed lines) and without (solid lines) ultra-thin films PMo_{12}. Electrolyte: 0.5 mol dm^{-3} H_2SO_4.

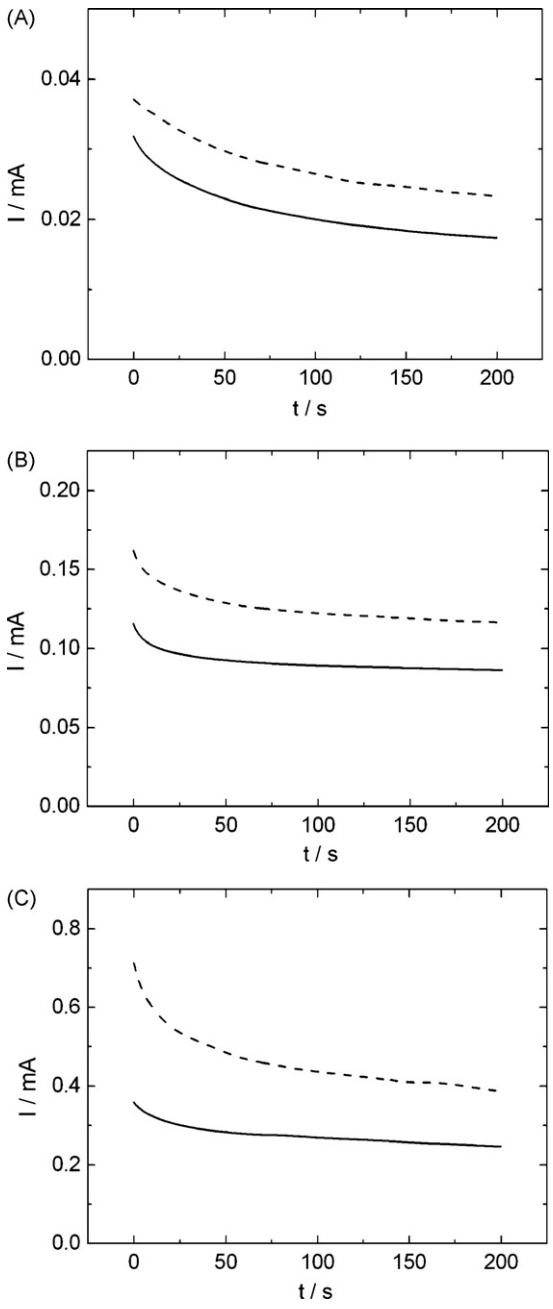

Fig. 5. Chronoamperometric responses recorded at 0.4 V. Other conditions as for Fig. 4.

nanoparticles (Fig. 6, solid line). Following measurements for 1 h, fairly stable steady-state current—potential responses have been observed. Further, the superior electrocatalytic activity of the modified systems (in comparison to the bare nanoparticles) has been retained. Some drop in the observed currents during prolonged measurements is caused by desorption of PMo_{12} adsorbates. The effect has been evident, indeed, when the catalytic material has been subjected (following the chronoamperometric measurement as for Fig. 6) to voltammetric cycling within the potential limits of Fig. 2C: the peaks characteristic of PMo_{12} have decreased ca. 15–20%.

The activating role of PMo_{12} may originate from the system's electroactivity (electron transfer mediating capabilities) at potentials up to ca. 0.5 V as well as from the possibility of donation of oxo groups by molybdates [37] or, more likely, through stabilization of such oxo species coming from the Ru or Sn components (that are known to induce oxidation of such poisoning species as carbon monoxide [4–7,12–15]). To explain high activity of PMo_{12}-modified Pt during oxygen reduction, it was postulated [21] that PMo_{12} molecules were sitting on platinum surface using only the outermost edge oxygen atoms; thus the adsorbate did not occupy (block) too many active platinum sites. Our present experiments are also consistent with the view that PMo_{12} does not block metallic platinum surface during oxidation of ethanol. Finally, it was also reported that the presence of molybdenum could increase catalytic activity of platinum towards electrooxidation of ethanol; indeed, the tri-metallic Pt–Ru–Mo system showed better performance than bimetallic Pt–Ru catalyst [38]. Interactions between platinum and molybdenum may result in changes of interfacial electronic struc-

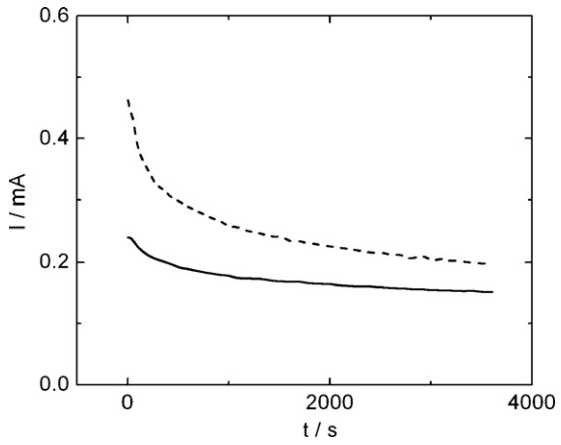

Fig. 6. Long-term chronoamperometric responses recorded at 0.4 V for the oxidation of 0.5 mol dm^{-3} ethanol at Pt–Sn/C nanoparticles covered with (dashed lines) and without (solid lines) ultra-thin films PMo_{12}. Electrolyte: 0.5 mol dm^{-3} H_2SO_4.

tures and thus affect adsorption force of carbon monoxide at the interface.

3.2.1. XPS probing of electronic interactions

In our mechanistic considerations, we concentrate here on the most efficient electrocatalytic system, namely on PMo_{12}-modified Pt–Sn. To comment on the electronic structure of the catalyst and on the promoting role of PMo_{12}, high-resolution XPS spectra have been collected for Pt 4*f* (Fig. 7) and Sn 3*d* (Fig. 8) core levels of the Pt–Sn/C catalytic system. In a case of PMo_{12}-modified sample, the Mo 3*d* signal is dominating, accounting for at least 75% Mo atomic percent, when compared to sum of Mo, Pt and Sn detected. No specific attenuation of the Pt 4*f*, Sn 3*d* and C 1*s* signals has been observed (Fig. 8), thus implying that PMo_{12} does not adsorb specifically on any of the above mentioned components of the catalyst. As carbon (Vulcan) support accounts for 80% of the catalyst's weight, we assume that most of PMo_{12} adsorbs on the latter substrate. Such explanation would be in agreement with the voltammetric data of Fig. 2.

The Pt 4*f* spectrum of the unmodified system (Fig. 7A) does not differ significantly from that obtained following exposure to PMo_{12} (Fig. 7B). Both spectra in Fig. 7 are typical for metallic nanosized Pt and for Pt in Pt-containing nanostructures [31,39]. The Sn 3*d* spectra have been deconvoluted into two doublets: with $3d_{5/2}$ component at 485.81 eV (lower oxidation state) and 486.94 eV (higher oxidation state), respectively (Fig. 8). Those oxidation states can be attributed either to metallic Sn (485.81 eV) and SnO (486.94 eV), or to SnO (485.81 eV) and SnO_2 (486.94 eV). No exact distinction is possible, because the reported BE ranges for Sn 3*d* peaks are broad and overlap in the cases of metallic Sn, SnO and SnO_2 [40,41]. The observed spin–orbit splitting for the Sn 3*d* signal is equal to 8.39 eV, and it is very close to the literature value of 8.41 eV [41].

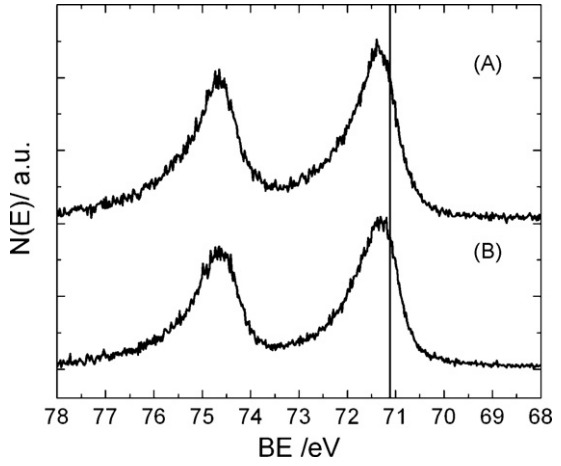

Fig. 7. XPS spectra of Pt 4*f* region recorded for (A) PMo_{12}-modified and (B) bare Vulcan-supported Pt–Sn nanoparticles. Shirley background corrected. Bulk Pt $4f_{7/2}$ electron energy (71.12 eV [37]) was marked using vertical line. Excitation energy: 650 eV.

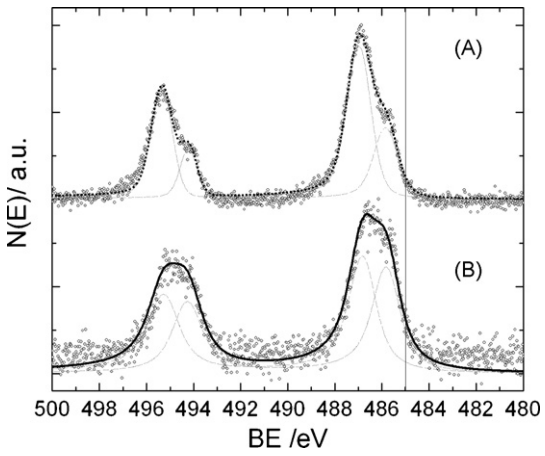

Fig. 8. Fit of XPS spectra recorded in the Sn 3*d* region for (A) PMo_{12}-modified and (B) bare Vulcan-supported Pt–Sn nanoparticles. Shirley background corrected. The spectra were deconvoluted into two doublets: for low Sn oxidation state with $3d_{5/2}$ component at 485.81 eV and for high Sn oxidation state, with $3d_{5/2}$ component at 486.94 eV (see text). Bulk Sn $3d_{5/2}$ electron energy (484.98 eV [37]) was marked using vertical line. Excitation energy: 650 eV.

It is apparent from our results that modification of the Pt–Sn nanoparticles with PMo_{12} decreases population of Sn in the lowest observed oxidation states (either metallic Sn or SnO, as discussed above). Deconvolution of Sn 3*d* spectra (Fig. 8) clearly shows that the population of Sn at the low oxidation states decreases from 52% (for unmodified Pt–Sn sample) to 30% for the sample obtained following modification with PMo_{12}. We can expect that this effect is caused by oxidative properties of PMo_{12} itself but it should be remembered that no reduction of Mo(VI) has been noticed in the XPS Mo 3*d* spectra (for the sake of clarity not shown here). It should be remembered that, in the case of PMo_{12}-modified Pt–Sn/C catalyst, PMo_{12} exists in relatively large amounts (relative to Sn). Further, close proximity of different Mo oxidation states in the Mo 3*d* spectra [40,41] can make their unequivocal distinction almost impossible. Consequently, determination of small amounts of possibly reduced Mo sites is below the detection limit and/or the resolution capabilities of the XPS setup used.

Based on XPS results, the high activity of the PMo_{12}-containing samples towards ethanol oxidation shall be thus attributed to the increased amounts of the oxidized forms of Sn. It was reported [30] that appearance of Sn oxides in Pt–Sn catalysts had an enhancement effect on electrooxidation of ethanol, and our present electrochemical results combined with the XPS data are consistent with this view. Most likely the existence of PMo_{12} in the vicinity of tin stabilizes higher oxidation states of Sn (presumably as tin oxo species). Otherwise bare tin oxides would readily be soluble in acid solutions.

4. Conclusions

Modification of Pt, Pt–Ru, and carbon (Vulcan)-supported Pt–Sn nanoparticles with ultra-thin films of PMo_{12} results in the enhancement of their electrocatalytic properties towards electrooxidation of ethanol, as demonstrated in terms of increases of the respective voltammetric and amperometric catalytic currents. The activation by PMo_{12} is the most effective in a case of Pt–Sn/C. It is notewor-

thy that such inorganic irreversibly adsorbed species as PMo_{12} are electroactive themselves and they may act as mediators of interfacial electron transfers during electrooxidation of ethanol. It cannot be excluded that molybdates (by analogy to Ru) may contribute to the bifunctional mechanism and, thus, provide oxo groups capable of removing the poisoning species (e.g. CO) from platinum surface. More likely, PMo_{12} interacts with ruthenium or tin oxo species in the bimetallic systems and acts as oxidizing and stabilizing agent. XPS data clearly imply that, in the presence of heteropolymolybdate, tin (in Pt–Sn) exists at higher oxidation states (presumably in a form of tin oxo species) when compared to the analogous PMo_{12}-free system.

On practical grounds, high activity of the proposed catalysts is restricted to a few (at least 3–4) hours of operation due to their limited stability (possibility of desorption of PMo_{12}). Further studies aiming at improvement of the systems' durability are in progress.

Acknowledgements

The support from Ministry of Science and Higher Education (Poland) under the grant Singapur/112/2007 is appreciated. A.L. was partially supported by University of Warsaw under grant BW-179208. The assistance by Gennady Cherkashinin, Eric Mankel and Thomas Mayer (TU Darmstadt) and Katarzyna Skorupska (HMI) during the beamtime, and Patrick Hoffmann and Dieter Schmeißer (BTU Cottbus) in running the beamline U49/2-PGM2 at Bessy-II (Berlin, Germany) is greatly appreciated. We are also indebted to Sascha Hümann and Peter Broekmann (University of Bonn, Germany) for their valuable contribution to the cell design, manufacture, and operation of the electrochemical setup.

References

[1] C. Lamy, S. Rousseau, E.M. Belgsir, C. Coutanceau, J.-M. Léger, Electrochim. Acta 49 (2004) 3901.
[2] H. Wang, Z. Jusys, R.J. Behm, J. Power Sources 154 (2006) 351.
[3] F.C. Simões, D.M. dos Anjos, F. Vigier, J.-M. Léger, F. Hahn, C. Coutanceau, E.R. Gonzalez, G. Tremiliosi-Filho, A.R. de Andrade, P. Olivi, K.B. Kokoh, J. Power Sources 167 (2007) 1.
[4] G. Tremiliosi-Filho, H. Kim, W. Chrzanowski, A. Wieckowski, B. Grzybowska, P. Kulesza, J. Electroanal. Chem. 467 (1999) 143.
[5] M. Watanabe, S. Motoo, J. Electroanal. Chem. 60 (1975) 267.
[6] A. Hamnett, Interfacial Electrochemistry—Theory Experiment and Applications, Marcel-Dekker, New York, 1999, pp. 871–873, Chapter 47.
[7] H.A. Gasteiger, N. Markovic, P.N. Ross, E.J. Cairns, J. Phys. Chem. 97 (1993) 12020.
[8] E. Antolini, J. Power Sources 170 (2007) 1.
[9] G.A. Camara, R.B. de Lima, T. Iwasita, Electrochem. Commun. 6 (2004) 812.
[10] J.P.I. de Souza, S.L. Queiroz, K. Bergamaski, E.R. Gonzalez, F.C. Nart, J. Phys. Chem. B 106 (2002) 9825.
[11] V. Pacheco Santos, V. Del Colle, R. Batista de Lima, G. Tremiliosi-Filho, Langmuir 20 (2004) 11064.
[12] A. Oliveira Neto, R.R. Dias, M.M. Tusi, M. Linardi, E.V. Spinacé, J. Power Sources 166 (2007) 87.
[13] S.Q. Song, W.J. Zhou, Z.H. Zhou, L.H. Jiang, G.Q. Sun, Q. Xin, V. Leontidis, S. Kontou, P. Tsiakaras, Int. J. Hydrogen Energy 30 (2005) 995.
[14] J. Mann, A.B. Nan Yao, Bocarsly, Langmuir 22 (2006) 10432.
[15] J.-M. Léger, S. Rousseau, C. Coutanceau, F. Hahn, C. Lamy, Electrochim. Acta 50 (2005) 5118.
[16] S. Song, P. Tsiakaras, Appl. Catal. B: Environ. 63 (2006) 187.
[17] T. Yamase, Chem. Rev. 98 (1998) 307.
[18] I.V. Kozhevnikov, Chem. Rev. 98 (1998) 171.
[19] M. Sadakane, E. Steckhan, Chem. Rev. 98 (1998) 219.
[20] M. Chojak, M. Mascetti, R. Wlodarczyk, R. Marassi, K. Karnicka, K. Miecznikowski, P.J. Kulesza, J. Solid-State Electrochem. 8 (2004) 854.
[21] M. Chojak, A. Kolary-Zurowska, R. Wlodarczyk, K. Miecznikowski, K. Karnicka, B. Palys, R. Marassi, P.J. Kulesza, Electrochim. Acta 52 (2007) 5574.
[22] P.J. Kulesza, M. Chojak, K. Karnicka, K. Miecznikowski, B. Palys, A. Lewera, A. Wieckowski, Chem. Mater. 16 (2004) 4128.
[23] R. Wlodarczyk, R. Marassi, M. Chojak, K. Miecznikowski, A. Kolary, P.J. Kulesza, J. Power Sources 159 (2006) 802.
[24] P.J. Kulesza, K. Karnicka, K. Miecznikowski, M. Chojak, A. Kolary, P.J. Barczuk, G. Tsirlina, W. Czerwiński, Electrochim. Acta 50 (2005) 5155.
[25] K. Karnicka, M. Chojak, K. Miecznikowski, M. Skunik, B. Baranowska, A. Kolary, A. Piranska, B. Palys, L. Adamczyk, P.J. Kulesza, Bioelectrochemistry 66 (2005) 79.
[26] D.M. Dos Anjos, K.B. Kokoh, J.M. Léger, A.R. De Andrade, P. Olivi, G. Tremiliosi-Filho, J. Appl. Electrochem. 36 (2006) 1391.
[27] A. Lewera, J. Inukai, W.P. Zhou, D. Cao, H.T. Duong, N. Alonso-Vante, A. Wieckowski, Electrochim. Acta 52 (2007) 5759.
[28] P.K. Babu, A. Lewera, J.H. Chung, R. Hunger, W. Jaegermann, N. Alonso-Vante, A. Wieckowski, E. Oldfield, J. Am. Chem. Soc. 129 (2007) 15140.
[29] S.Q. Song, W.J. Zhou, Z.H. Zhou, L.H. Jiang, G.Q. Sun, P. Tsiakaras, Q. Xin, V. Leonditis, S. Kontou, P. Tsiakaras, Int. J. Hydrogen Energy 30 (2005) 995.
[30] L. Jiang, G. Sun, S. Sun, J. Liu, S. Tang, H. Li, B. Zhou, Q. Xin, Electrochim. Acta 50 (2005) 5384.
[31] A. Lewera, W.P. Zhou, C. Vericat, J.H. Chung, R. Haasch, A. Wieckowski, P.S. Bagus, Electrochim. Acta 51 (2006) 3950.
[32] A. Lewera, M. Chojak, K. Miecznikowski, P.J. Kulesza, Electroanalysis 17 (2005) 1471.
[33] P.J. Kulesza, M. Skunik, B. Baranowska, K. Miecznikowski, M. Chojak, K. Karnicka, E. Frackowiak, F. Béguin, A. Kuhn, M.H. Delville, B. Starobrzynska, A. Ernst, Electrochim. Acta 51 (2006) 2373.
[34] P. Garrigue, M.-H. Delville, C. Labrugère, E. Cloutet, P.J. Kulesza, J.P. Morand, A. Kuhn, Chem. Mater. 16 (2004) 2984.
[35] M. Skunik, M. Chojak, I.A. Rutkowska, P.J. Kulesza, Electrochim. Acta 53 (2008) 3862.
[36] M. Skunik, B. Baranowska, D. Fattakhova, K. Miecznikowski, M. Chojak, A. Kuhn, P.J. Kulesza, J. Solid-State Electrochem. 10 (2006) 168.
[37] A. Lima, C. Coutanceau, J.-M. Léger, C. Lamy, J. Appl. Electrochem. 31 (2001) 379.
[38] A. Oliveira Neto, E.G. Franco, E. Aricó, M. Linardi, E.R. Gonzalez, J. Eur. Ceram. Soc. 23 (2003) 2987.
[39] W.P. Zhou, A. Lewera, P.S. Bagus, A. Wieckowski, J. Phys. Chem. C 111 (2007) 13490.
[40] C.D. Wagner, A.V. Naumkin, A. Kraut-Vass, J.W. Allison, C.J. Powell, J.R. Rumble Jr, NIST X-ray Photoelectron Spectroscopy Database. NIST Standard Reference Database 20, Version 3. 5 (web version), 2007.
[41] J.F. Moulder, W.F. Stickle, P.E. Sobol, K.D. Bomben, Handbook of X-ray Photoelectron Spectroscopy. A Reference Book of Standard Spectra for Identification and Interpretation of XPS Spectra, Physical Electronic, Inc., Eden Praire, MN, USA, 1995.